



23 analysis is required in order to use the satellite differential method in inverse modeling of NO_x
24 emissions.

25

26 **1. Introduction**

27 Nitrogen oxides (NO_x=NO+NO₂) play an important role in tropospheric photochemistry of
28 ozone and secondary aerosol formation. There are normally emitted from both anthropogenic (e.g.,
29 fossil fuel combustion) and natural sources (e.g., lightning, soil, and wild fire). The rapid economic
30 growth in East Asia has led to a significant increase of energy consumptions and thereby
31 anthropogenic NO_x emissions during last two decades (Ghude et al., 2009; Gu et al., 2013; Ma et
32 al., 2006; Mijling et al., 2013; Richter et al., 2005; Stavrakou et al., 2008; van der A et al., 2006;
33 Zhang et al., 2007).

34 The traditional bottom-up emission inventory rely on detailed information about sources and
35 emission factors and therefore can have large uncertainties especially in countries such as China
36 where the emission information is incomplete (Streets et al., 2003). In recent years, satellite
37 measurements of nitrogen dioxide (NO₂) from multiple instruments, including Global Ozone
38 Monitoring Experiment (GOME), Scanning Imaging Absorption Spectrometer for Atmospheric
39 Cartography (SCIAMACHY), Ozone Monitoring Instrument (OMI) and GOME-2, have been
40 widely used to derive top-down estimation of NO_x emissions as an alternative to the bottom-up
41 emission inventory (Gu et al., 2014; Jaegle et al., 2005; Lamsal et al., 2011; Lin et al., 2010;
42 Stavrakou et al., 2008; Zhang et al., 2012).

43 Inverse modeling of NO_x emissions, incorporating model simulations and satellite observations,
44 can help reduce uncertainties in bottom-up inventories especially in China (Lin et al., 2012;
45 Mijling and van der A, 2012; Zhao and Wang, 2009). Martin et al. (2003) developed the first



46 monthly inversion method by scaling the bottom-up emission inventory with top-down constraints
47 from GOME NO₂ column measurements. Zhao and Wang (2009) improved the method by
48 carrying out the emission inversion iteratively on a daily basis. Gu et al. (2014) further refined this
49 method by including column NO₂ retrieval in inverse modeling, which removes the biases
50 introduced by inconsistency between NO₂ profiles in the retrieval and inverse modeling. Lin et al.
51 (2010) developed a method of inverse modeling using column NO₂ difference between GOME-2
52 and OMI.

53 In the emission inversion problem, the a posteriori emission is estimated by modifying the a
54 priori emission with a term proportional to the difference between the simulated and observed
55 column density, which can be expressed as:

$$56 \quad E = E_a + \alpha \times (\Omega_s - \Omega_m) \quad (1)$$

57 where E is the a posteriori emission, E_a is the a priori emission used in model simulation, Ω_s is
58 satellite observed column, Ω_m is model simulated column and α is the correction rate. In the
59 original formulation by Martin et al. (2003) and all subsequent studies using this or some variants
60 of this method (Jaegle et al., 2005; Lamsal et al., 2011), α is calculated as the ratio between the a
61 priori emission and simulated column (referred to as the bulk ratio hereafter):

$$62 \quad \alpha = E_a / \Omega_m \quad (2)$$

63 Note that this formulation has an implicit assumption that the emission is linearly proportional to
64 the column density. However, previous studies of the emission and column trends suggested that
65 the nonlinearity between NO_x emission and tropospheric NO₂ column is non-trivial (Gu et al.,
66 2013; Lamsal et al., 2011; Lu and Streets, 2012; Stavrou et al., 2008). This nonlinear relationship
67 is mainly due to the nonlinear photochemical feedbacks between NO_x and OH (the increase in NO_x
68 promotes OH production and reduces its lifetime in the low-emission condition, but suppresses



69 OH production and increases its lifetime in the high-emission condition). Figure 1 shows
70 tropospheric NO₂ column densities as a function of surface emissions at GOME-2 and OMI
71 overpass time over eastern China simulated in the Regional chEmical and trAnsport Model
72 (REAM) (model details are given in section 2.2). Clearly tropospheric NO₂ column is not linearly
73 proportional to NO_x emission, which was assumed in Eq. (2). The difference in the nonlinearity in
74 the ratio of emission to column NO₂ between GOME-2 and OMI overpass time reflects in part the
75 difference in the relative importance between transport and chemistry at different time of a day.

76 In this study, we examine if considering the nonlinear ratio between NO_x emissions and NO₂
77 columns can improve the inverse modeling results and reduce the discrepancies in emission
78 estimates using different satellite observations. Applying Taylor expansion to Eq. (1), we define a
79 local derivative in place of the bulk ratio (Eq. (2)). We implement the local derivative of emission
80 to column NO₂ ratio in the REAM model and examine its effects on the inverse modeling estimates
81 of surface anthropogenic NO_x emissions with GOME-2 and OMI measurements over China in
82 August 2007. The new inversion results are compared to those using the bulk ratio method and the
83 satellite differential method (Lin et al., 2010) and the implications for NO_x inverse modeling are
84 discussed.

85

86 **2. Satellite data and inverse modeling method**

87 **2.1 Satellite data**

88 We use the measurements from GOME-2 and OMI instruments in this study. Both instruments
89 are nadir-viewing spectrometers (Boersma et al., 2004; 2011; 2007). The OMI instrument was
90 launched onboard the Aura satellite in July 2004, and it has a spatial resolution of $24 \times 13 \text{ km}^2$ at
91 nadir (Levelt et al., 2006). The GOME-2 instrument was launched onboard the MetOp satellite in



92 June 2006 with ground pixel size of $80 \times 40 \text{ km}^2$ (Irie et al., 2012). The local overpass time across
93 the equator is around 9:30 for GOME-2 and around 13:30 for OMI. We use the Royal Netherlands
94 Meteorological Institute (KNMI) OMI (DOMINO2 v2.0) and GOME-2 (TM4NO2A v2.3)
95 tropospheric NO_2 vertical column density (VCD) products for this study. We excluded the data
96 flagged with row anomalies from the OMI measurements
97 (<http://www.knmi.nl/omi/research/product/rowanomaly-background.php>). To reduce the cloud
98 interference, we only use measured NO_2 column data when cloud fraction is $< 20\%$ for both
99 measurements.

100 The error in the retrieval of NO_2 tropospheric VCD is determined by those in total slant column
101 density (SCD), stratospheric SCD, and tropospheric air mass factor (AMF) estimation. In this
102 study, we use total and stratospheric SCD errors from KNMI DOMINO2 and TM4NO2A products,
103 and compute the uncertainty of tropospheric AMF estimation following the KNMI algorithm. The
104 details of error analysis were described by Boersma et al. (2004; 2011; 2007) and Hains et al.
105 (2010). In general, the uncertainties of total and stratospheric SCD estimations are small
106 ($< 0.7 \times 10^{15} \text{ molec. cm}^{-2}$) relative to high tropospheric VCDs over eastern China (Zhao and Wang,
107 2009). The uncertainty in tropospheric AMF comes from surface albedo, cloud fraction, cloud
108 pressure, and profile shape. The uncertainty from a priori profile can lead to $\sim 10\%$ error in
109 tropospheric VCD retrievals. The total uncertainty of an individual retrieval is up to 50% over
110 highly polluted eastern China for both OMI and GOME-2.

111

112 **2.2 REAM model**

113 The 3-D REAM has been applied in a number of tropospheric chemistry and transport studies
114 over East Asia, North America and polar regions (Choi et al., 2008a; Choi et al., 2008b; Choi et



115 al., 2005; Gu et al., 2014; Gu et al., 2013; Jing et al., 2006; Liu et al., 2012a; Liu et al., 2012b; Liu
116 et al., 2010; Wang et al., 2007; Wang et al., 2006; Yang et al., 2011; Zeng et al., 2006; Zeng et al.,
117 2003; Zhao et al., 2009a; Zhao et al., 2010; Zhao et al., 2009b). The model has a horizontal
118 resolution of $36 \times 36 \text{ km}^2$ with 30 vertical layers in the troposphere. Transport is driven by WRF
119 assimilated meteorological fields constrained by the NCEP reanalysis products
120 (<http://www.esrl.noaa.gov/psd/>). The chemistry mechanism in the REAM is adopted from the
121 GEOS-Chem model (Bey et al., 2001) with updates of kinetics data
122 (<http://jpldataeval.jpl.nasa.gov/>). The anthropogenic NO_x and VOCs emissions are from Zhang et
123 al. (2009). The biomass burning emissions are taken from the Global Fire Emissions Database,
124 Version 2 (GFEDv2.1; available at <http://daac.ornl.gov/>). The lightning NO_x emission is
125 parameterized as in Zhao et al. (2010).

126

127 **2.3 Inverse modeling method**

128 As discussed in the introduction, the bulk ratio (α) used in the traditional method is based on
129 the assumption of a linear relationship between NO_x emission and tropospheric column NO_2 ,
130 which is only accurate under a low emission condition. As shown in Figure 1, using the bulk ratio
131 for inverse modeling overlooks the nonlinear chemical feedback of NO_x lifetime at different
132 satellite overpass time, which not only affects the accuracy of inverse modeling results but also
133 leads to inconsistency between emission inversions using different satellite measurements. To
134 account for the nonlinearity, we apply Taylor expansion to Eq. (1) and obtain a local derivative
135 ratio (α^*) to replace Eq. (2):

$$136 \quad \alpha^* = \Delta E_a / \Delta \Omega_m \quad (3)$$

137 where ΔE_a is the change of the a priori emission and $\Delta \Omega_m$ is the change of model simulated column.



138 The Taylor expansion formulation of Eqs. (1) and (3) is equivalent to the previous works
139 by Vinken et al. (2014a; 2014b) and Castellanos et al. (2014), who accounted for the nonlinear
140 chemistry effect by adding the ratio of relative emission to relative column NO₂ changes, first
141 introduced by Lamsal et al. (2011), to the formulation of Eqs. (1) and (2). For inversion of ship
142 emissions, Vinken et al. (2014b) computed averaged nonlinear factors for selected regions with
143 perturbations proportional to model-observation column difference. They also added a correction
144 of profile change in their formulation. For polluted regions, the effect of profile change is small
145 (Zhang et al., 2016) and is not included in this study. In the previous studies, model sensitivities
146 are computed with domain-wide emission perturbations. This approach introduces uncertainties
147 since the column change in a given grid cell is affected by emission changes in both that grid cell
148 and upwind grid cells; the effects of upwind grid cells are a complex function of emissions,
149 chemistry, and transport. As in Gu et al. (2013), we carried out single-cell based emission
150 perturbation in the 3-D REAM model to compute the value of α^* . We first archived the 3-D
151 influxes of all model tracers at each time step in the standard simulation. In the perturbation
152 simulation (15% of anthropogenic NO_x emissions), the influxes of all model tracers for all grid
153 cells were replaced with the archived values at each time step. Consequently the emission
154 perturbation only affects NO_x chemistry, out flux, and concentration in the same grid cell. Using
155 the perturbation and standard simulation results, we computed the value of α^* and applied it to Eq.
156 (1) to estimate inversed NO_x emission over eastern China in August 2007 with either GOME-2 or
157 OMI observations. The results from the local derivative method are compared with those using the
158 bulk ratio method in later sections.

159 The uncertainties of the a posteriori emissions come from those in a priori and top-down
160 emission estimates. Uncertainties in top-down emission estimates are derived from those in



161 tropospheric NO₂ VCD retrievals and model simulations. The retrieval uncertainty is discussed in
162 section 2.1. The uncertainty of model simulation is estimated at 30% and that of the bottom-up
163 inventory is ~60% over China (Zhao and Wang, 2009). The overall uncertainty of the a posteriori
164 emission is typically in the range of 20-40% over polluted eastern China.

165

166 **3. Results and discussion**

167 **3.1 Comparisons between α and α^***

168 Figure 2 compares the relative difference between local derivative ratio (α^*) and bulk ratio (α)
169 values over eastern China for August 2007, at GOME-2 and OMI overpass time, respectively. For
170 both satellites, α^* is higher (>20%) than α over most low-emission rural regions but lower (-20--
171 60%) than α over most high-emission regions including eastern coastal areas and Sichuan
172 Province. For emission estimates, the inversion biases over high emission regions tend to be more
173 important than rural regions. The high bias of α relative to α^* implies that top-down NO_x emission
174 estimates tend to over-correct for a given difference between observed and simulated column NO₂.
175 We note here that the inversion bias can be either positive or negative depending on the column
176 difference.

177

178 **3.2 NO_x emission inversion consistency between OMI and GOME-2**

179 Another way to look at the effects of correction biases using the bulk ratio relative to local
180 derivative method is to compare the inversion estimated NO_x emissions using OMI and GOME-2
181 measurements. Gu et al. (2014) showed that inversion results using standard DOMINO products
182 of GOME-2 tend to be higher than OMI due possibly to a bias in the TM4 NO₂ profiles used in
183 GOME-2 retrievals. Coupling this tendency of a high retrieval bias of GOME-2 with the different



184 sensitivities discussed in the previous paragraph implies that the bulk ratio formulation would
185 tends to overcorrect and estimate higher NO_x emissions using GOME-2 than OMI measurements
186 in polluted regions.

187 The bias expectation is confirmed in Figure 3. While the inversion results using DOMINO
188 GOME-2 and OMI products show in general higher NO_x emissions in the former, the difference
189 between the inversions using two satellites is smaller using the local derivative than bulk ratio
190 method, particularly over high emission regions. For example, we compare the emission estimates
191 between the bulk ratio and local derivative methods in three largest megacities in China (e.g.
192 Beijing, Shanghai and Guangzhou). Using the bulk ratio method, the relative difference of
193 inversion emission estimates of using two satellites products relative to OMI results are 54.2%,
194 70.5% and 55.6% for the three megacities, respectively. The local derivative method reduces the
195 corresponding relative difference down to 9.0%, 5.3% and 13.5%, respectively (Figure 3 and Table
196 1). These results demonstrate that a significant fraction of the discrepancy in inversed NO_x
197 emissions between different instruments can be attributed to neglecting the chemical nonlinearity
198 in the traditional bulk ratio method and that improvement can be achieved with the local derivative
199 method that we proposed in this study. The remaining discrepancy between inversion emission
200 estimates using GOME-2 and OMI observations is likely due to NO₂ profiles used in the retrieval
201 and possible systematic biases between the two satellite instruments (Gu et al., 2014).

202

203 **3.3 Comparison of inversion results between using the bulk ratio method and the satellite** 204 **differential approach**



205 With column NO₂ measurements from two satellites, Lin et al. (2010) developed a method to
 206 utilize information from two different satellites (referred to as the satellite differential method in
 207 this study) to improve the emission estimates. The formulation of the method is as follows,

$$208 \quad \frac{E_j}{E_a} = \frac{\Omega_{OMI} - \Omega_{GOME-2} \cdot \exp(-t/\tau)}{\Omega_{m1330} - \Omega_{m0930} \cdot \exp(-t/\tau)} \quad (4)$$

209 where E_j is the a posteriori emission, E_a is the a priori emission, Ω_{OMI} is OMI observed NO₂ column,
 210 Ω_{GOME-2} is GOME-2 observed NO₂ column, Ω_{m1330} is model simulated NO₂ column at OMI
 211 overpass time, Ω_{m0930} is model simulated NO₂ column at GOME-2 overpass time, t is the time gap
 212 between two satellite overpass time, and τ is the lifetime of NO_x. The derivation of this method is
 213 analogous to the bulk ratio method (Lin et al., 2010) and is not directly comparable to the local
 214 derivative method. We therefore compare the inversion results using the satellite differential
 215 method with those using the bulk ratio method.

216 In Table 1, the inversion emission estimates using the satellite differential method are compared
 217 with those using the bulk ratio method over eastern China in August 2007. As discussed in the
 218 previous section, the bulk ratio method leads to consistently high emission estimates using GOME-
 219 2 products compared to using OMI over high emission ratios, e.g., 50-70% in the three megacities.
 220 The estimates using the satellite differential method are even lower than the bulk ratio inversion
 221 estimates using OMI products. The reason is that in our analysis $\Omega_{GOME-2}/\Omega_{m0930}$ is consistently
 222 larger than $\Omega_{OMI}/\Omega_{m1330}$ over eastern China (Figure 4). The mathematical analysis in Appendix A
 223 shows that consequently a posteriori emission estimates using the satellite differential method are
 224 consistently lower than that using the bulk ratio method with either GOME-2 or OMI products.
 225 When the differences between the two satellite products are not well characterized, we find that
 226 the local derivative method is more robust relative to the bulk ratio and satellite differential
 227 methods (Table 1).



228

229 **4. Conclusions**

230 We show in this study that the nonlinearity of NO_x chemistry implies that the local
231 derivative (of a first-order Taylor expansion) is better suited in the inversion formulation
232 developed by Martin et al. (2003) than bulk ratio, in agreement with Vinken et al. (2014a; 2014b)
233 and Castellanos et al. (2014). In this study, single grid cell based perturbation sensitivity
234 calculation was used instead of previous domain-wide perturbations such that upwind emission
235 changes do not affect local derivative estimates. The latter effects can be more appropriately
236 accounted for using the iterative method by Zhao and Wang (2009) and Gu et al. (2014). In the
237 context of the inversion formulation by Martin et al. (2003), we compared the bulk-ratio and local
238 derivative methods in inverting modeling of anthropogenic NO_x emissions over eastern China for
239 August 2007. At the observation time of OMI and GOME-2, the local derivative ratios (α^*) are
240 smaller (-20~-60%) than the bulk ratios (α) over most high-emission regions, but are higher
241 (>20%) than bulk ratios (α) over most low-emission rural regions. Over high emission regions, the
242 inversion emission estimates using the local derivative method produces more consistent results
243 between OMI and GOME-2 products than the bulk ratio method. In our work, the observed to
244 simulated tropospheric column NO₂ are consistently higher for GOME-2 than OMI over high
245 emission regions of eastern China, leading to a consistent low bias in a posteriori emission
246 estimates by the satellite differential method relative to those by the other methods.
247 Computationally, the local derivative ratio is more complex to compute than bulk ratio. The
248 iterative method in the previous work by Zhao and Wang (2009) and Gu et al. (2014) can largely
249 mitigate the biases introduced by the bulk ratio method, although the inversion convergence time
250 will likely be reduced when using local derivative than bulk ratios. For certain applications such



251 as deriving the timeline of emission reduction during the Beijing Olympics (Yang et al., 2011),
252 reducing the inversion convergence time is critically important. Further studies are needed to
253 quantify the improvements.

254

255 **Acknowledgements**

256 This work was supported by the NSF Atmospheric Chemistry and NASA ACMAP Programs.
257 We acknowledge the free use of OMI and GOME-2 data and products from www.temis.nl. We
258 thank Folkert Boersma for his suggestions.

259

260 **Appendix A**

261 Table 1 shows that the inversion results using the satellite differential method are
262 consistently lower than that of the bulk ratio method using OMI measurements, which are lower
263 than the bulk ratio method using GOME-2 measurements over high emission regions. Here we
264 show the mathematical analysis demonstrating the reasons for the consistent difference. In our
265 analysis, the following inequality is found over high emission regions of eastern China (Figure 4),

$$266 \quad \frac{\Omega_{\text{GOME-2}}}{\Omega_{m930}} - \frac{\Omega_{\text{OMI}}}{\Omega_{m1330}} > 0 \quad (\text{A1})$$

267 It follows that

$$268 \quad \Omega_{\text{GOME-2}}\Omega_{m1330} - \Omega_{\text{OMI}}\Omega_{m930} > 0$$

269 Therefore,

$$270 \quad \Omega_{\text{OMI}}\Omega_{m1330} - \Omega_{\text{OMI}}\Omega_{m930}\exp\left(-\frac{t}{\tau}\right) > \Omega_{\text{OMI}}\Omega_{m1330} - \Omega_{\text{GOME-2}}\Omega_{m1330}\exp\left(-\frac{t}{\tau}\right)$$

271 and

$$272 \quad \frac{\Omega_{\text{OMI}}\Omega_{m1330} - \Omega_{\text{GOME-2}}\Omega_{m1330}\exp\left(-\frac{t}{\tau}\right)}{\Omega_{\text{OMI}}\Omega_{m1330} - \Omega_{\text{OMI}}\Omega_{m930}\exp\left(-\frac{t}{\tau}\right)} < 1$$



273 We obtain,

$$274 \quad \frac{\Omega_{\text{OMI}} - \Omega_{\text{GOME-2}} \exp\left(-\frac{t}{\tau}\right)}{\Omega_{m1330} - \Omega_{m930} \exp\left(-\frac{t}{\tau}\right)} < \frac{\Omega_{\text{OMI}}}{\Omega_{m1330}} < \frac{\Omega_{\text{GOME-2}}}{\Omega_{m930}} \quad (\text{A2})$$

275

276 Given a priori emission estimation of Eq. (2) and (4), Eq. (A2) implies that

$$277 \quad E_j < E_{b,\text{OMI}} < E_{b,\text{GOME-2}} \quad (\text{A3})$$

278 where E_j is the inversion emission estimate by the satellite differential method, $E_{b,\text{OMI}}$ is the

279 inversion emission estimate by the bulk ratio method using OMI measurements, and $E_{b,\text{GOME-2}}$ is

280 the inversion emission estimate by the bulk ratio method using GOME-2 measurements.

281

282 References

283 Bey, I., Jacob, D. J., Yantosca, R. M., Logan, J. A., Field, B. D., Fiore, A. M., Li, Q. B., Liu, H.

284 G. Y., Mickley, L. J., and Schultz, M. G.: Global modeling of tropospheric chemistry with

285 assimilated meteorology: Model description and evaluation, *Journal of Geophysical Research-*

286 *Atmospheres*, 106, 23073-23095, 2001.

287 Boersma, K. F., Eskes, H. J., and Brinksma, E. J.: Error analysis for tropospheric NO₂ retrieval

288 from space, *J. Geophys. Res.*, 109, D04311, 2004.

289 Boersma, K. F., Eskes, H. J., Dirksen, R. J., van der A, R. J., Veefkind, J. P., Stammes, P., Huijnen,

290 V., Kleipool, Q. L., Sneep, M., Claas, J., Leitão, J., Richter, A., Zhou, Y., and Brunner, D.: An

291 improved tropospheric NO₂ column retrieval algorithm for the Ozone Monitoring Instrument,

292 *Atmospheric Measurement Techniques*, 4, 1905-1928, 2011.

293 Boersma, K. F., Eskes, H. J., Veefkind, J. P., Brinksma, E. J., van der A, R. J., Sneep, M., van den

294 Oord, G. H. J., Levelt, P. F., Stammes, P., Gleason, J. F., and Bucsela, E. J.: Near-real time retrieval

295 of tropospheric NO₂ from OMI, *Atmospheric Chemistry and Physics*, 7, 2103-2118, 2007.



- 296 Castellanos, P., Boersma, K. F., and van der Werf, G. R.: Satellite observations indicate substantial
297 spatiotemporal variability in biomass burning NO_x emission factors for South America, Atmos.
298 Chem. Phys., 14, 3929-3943, 2014.
- 299 Choi, Y., Wang, Y., Zeng, T., Cunnold, D., Yang, E. S., Martin, R., Chance, K., Thouret, V., and
300 Edgerton, E.: Springtime transitions of NO₂, CO, and O₃ over North America: Model evaluation
301 and analysis, Journal of Geophysical Research-Atmospheres, 113, 2008a.
- 302 Choi, Y., Wang, Y. H., Yang, Q., Cunnold, D., Zeng, T., Shim, C., Luo, M., Eldering, A., Bucsel, E.,
303 and Gleason, J.: Spring to summer northward migration of high O₃ over the western North
304 Atlantic, Geophysical Research Letters, 35, 2008b.
- 305 Choi, Y., Wang, Y. H., Zeng, T., Martin, R. V., Kurosu, T. P., and Chance, K.: Evidence of
306 lightning NO_x and convective transport of pollutants in satellite observations over North America,
307 Geophysical Research Letters, 32, 2005.
- 308 Ghude, S. D., Van der A, R. J., Beig, G., Fadnavis, S., and Polade, S. D.: Satellite derived trends
309 in NO₂ over the major global hotspot regions during the past decade and their inter-comparison,
310 Environ. Pollut., 157, 1873-1878, 2009.
- 311 Gu, D., Wang, Y., Smeltzer, C., and Boersma, K. F.: Anthropogenic emissions of NO_x over China:
312 Reconciling the difference of inverse modeling results using GOME-2 and OMI measurements,
313 Journal of Geophysical Research: Atmospheres, doi: 10.1002/2014JD021644, 2014.
314 2014JD021644, 2014.
- 315 Gu, D., Wang, Y., Smeltzer, C., and Liu, Z.: Reduction in NO_x Emission Trends over China:
316 Regional and Seasonal Variations, Environ. Sci. Technol., 47, 12912-12919, 2013.
- 317 Hains, J. C., Boersma, K. F., Kroon, M., Dirksen, R. J., Cohen, R. C., Perring, A. E., Bucsel, E.,
318 Volten, H., Swart, D. P. J., Richter, A., Wittrock, F., Schoenhardt, A., Wagner, T., Ibrahim, O. W.,
319 van Roozendaal, M., Pinardi, G., Gleason, J. F., Veefkind, J. P., and Levelt, P.: Testing and
320 improving OMI DOMINO tropospheric NO₂ using observations from the DANDELIONS and
321 INTEX-B validation campaigns, Journal of Geophysical Research: Atmospheres, 115, D05301,
322 2010.



- 323 Irie, H., Boersma, K. F., Kanaya, Y., Takashima, H., Pan, X., and Wang, Z. F.: Quantitative bias
324 estimates for tropospheric NO₂ columns retrieved from SCIAMACHY, OMI, and GOME-2 using
325 a common standard for East Asia, *Atmospheric Measurement Techniques*, 5, 2403-2411, 2012.
- 326 Jaegle, L., Steinberger, L., Martin, R. V., and Chance, K.: Global partitioning of NO_x sources using
327 satellite observations: Relative roles of fossil fuel combustion, biomass burning and soil emissions,
328 *Faraday Discussions*, 130, 407-423, 2005.
- 329 Jing, P., Cunnold, D., Choi, Y., and Wang, Y.: Summertime tropospheric ozone columns from
330 Aura OMI/MLS measurements versus regional model results over the United States, *Geophysical
331 Research Letters*, 33, 2006.
- 332 Lamsal, L. N., Martin, R. V., Padmanabhan, A., van Donkelaar, A., Zhang, Q., Sioris, C. E.,
333 Chance, K., Kurosu, T. P., and Newchurch, M. J.: Application of satellite observations for timely
334 updates to global anthropogenic NO_x emission inventories, *Geophysical Research Letters*, 38,
335 L05810, 2011.
- 336 Levelt, P. F., Hilsenrath, E., Leppelmeier, G. W., van den Oord, G. H. J., Bhartia, P. K., Tamminen,
337 J., de Haan, J. F., and Veefkind, J. P.: Science objectives of the Ozone Monitoring Instrument, *Ieee
338 Transactions on Geoscience and Remote Sensing*, 44, 1199-1208, 2006.
- 339 Lin, J. T., Liu, Z., Zhang, Q., Liu, H., Mao, J., and Zhuang, G.: Modeling uncertainties for
340 tropospheric nitrogen dioxide columns affecting satellite-based inverse modeling of nitrogen
341 oxides emissions, *Atmospheric Chemistry and Physics*, 12, 12255-12275, 2012.
- 342 Lin, J. T., McElroy, M. B., and Boersma, K. F.: Constraint of anthropogenic NO_x emissions in
343 China from different sectors: a new methodology using multiple satellite retrievals, *Atmospheric
344 Chemistry and Physics*, 10, 63-78, 2010.
- 345 Liu, Z., Wang, Y., Gu, D., Zhao, C., Huey, L. G., Stickel, R., Liao, J., Shao, M., Zhu, T., Zeng, L.,
346 Amoroso, A., Costabile, F., Chang, C. C., and Liu, S. C.: Summertime photochemistry during
347 CAREBeijing-2007: RO_x budgets and O₃ formation, *Atmospheric Chemistry and Physics*, 12,
348 7737-7752, 2012a.



- 349 Liu, Z., Wang, Y., Vrekoussis, M., Richter, A., Wittrock, F., Burrows, J. P., Shao, M., Chang, C.-
350 C., Liu, S.-C., Wang, H., and Chen, C.: Exploring the missing source of glyoxal (CHOCHO) over
351 China, *Geophysical Research Letters*, 39, 2012b.
- 352 Liu, Z., Wang, Y. H., Gu, D. S., Zhao, C., Huey, L. G., Stickel, R., Liao, J., Shao, M., Zhu, T.,
353 Zeng, L. M., Liu, S. C., Chang, C. C., Amoroso, A., and Costabile, F.: Evidence of Reactive
354 Aromatics As a Major Source of Peroxy Acetyl Nitrate over China, *Environ. Sci. Technol.*, 44,
355 7017-7022, 2010.
- 356 Lu, Z. and Streets, D. G.: Increase in NO_x Emissions from Indian Thermal Power Plants during
357 1996–2010: Unit-Based Inventories and Multisatellite Observations, *Environ. Sci. Technol.*, doi:
358 10.1021/es300831w, 2012. 2012.
- 359 Ma, J. Z., Richter, A., Burrows, J. P., Nuss, H., and van Aardenne, J. A.: Comparison of model-
360 simulated tropospheric NO₂ over China with GOME-satellite data, *Atmospheric Environment*, 40,
361 593-604, 2006.
- 362 Martin, R. V., Jacob, D. J., Chance, K., Kurosu, T. P., Palmer, P. I., and Evans, M. J.: Global
363 inventory of nitrogen oxide emissions constrained by space-based observations of NO₂ columns,
364 *Journal of Geophysical Research-Atmospheres*, 108, 2003.
- 365 Mijling, B. and van der A, R. J.: Using daily satellite observations to estimate emissions of short-
366 lived air pollutants on a mesoscopic scale, *J. Geophys. Res.*, 117, D17302, 2012.
- 367 Mijling, B., van der A, R. J., and Zhang, Q.: Regional nitrogen oxides emission trends in East Asia
368 observed from space, *Atmos. Chem. Phys. Discuss.*, 13, 17519-17544, 2013.
- 369 Richter, A., Burrows, J. P., Nuss, H., Granier, C., and Niemeier, U.: Increase in tropospheric
370 nitrogen dioxide over China observed from space, *Nature*, 437, 129-132, 2005.
- 371 Stavrou, T., Muller, J. F., Boersma, K. F., De Smedt, I., and van der A, R. J.: Assessing the
372 distribution and growth rates of NO_x emission sources by inverting a 10-year record of NO₂
373 satellite columns, *Geophysical Research Letters*, 35, 5, 2008.



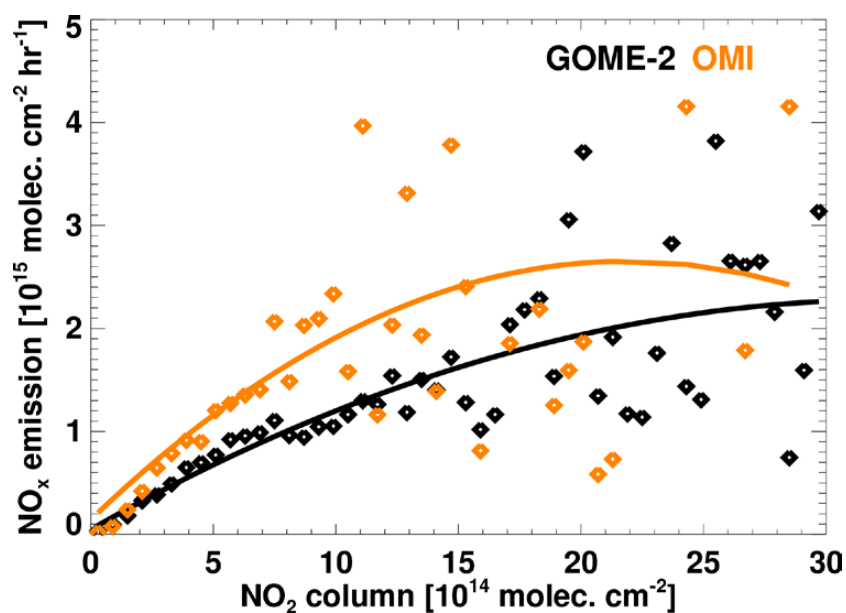
- 374 Streets, D. G., Bond, T. C., Carmichael, G. R., Fernandes, S. D., Fu, Q., He, D., Klimont, Z.,
375 Nelson, S. M., Tsai, N. Y., Wang, M. Q., Woo, J. H., and Yarber, K. F.: An inventory of gaseous
376 and primary aerosol emissions in Asia in the year 2000, *Journal of Geophysical Research-*
377 *Atmospheres*, 108, 2003.
- 378 van der A, R. J., Peters, D., Eskes, H., Boersma, K. F., Van Roozendaal, M., De Smedt, I., and
379 Kelder, H. M.: Detection of the trend and seasonal variation in tropospheric NO₂ over China,
380 *Journal of Geophysical Research-Atmospheres*, 111, 10, 2006.
- 381 Vinken, G. C. M., Boersma, K. F., Maasakkers, J. D., Adon, M., and Martin, R. V.: Worldwide
382 biogenic soil NO_x emissions inferred from OMI NO₂ observations, *Atmos. Chem. Phys.*, 14,
383 10363-10381, 2014a.
- 384 Vinken, G. C. M., Boersma, K. F., van Donkelaar, A., and Zhang, L.: Constraints on ship NO_x
385 emissions in Europe using GEOS-Chem and OMI satellite NO₂ observations, *Atmos. Chem. Phys.*,
386 14, 1353-1369, 2014b.
- 387 Wang, Y., Choi, Y., Zeng, T., Davis, D., Buhr, M., Huey, L. G., and Neff, W.: Assessing the
388 photochemical impact of snow NO_x emissions over Antarctica during ANTCI 2003, *Atmospheric*
389 *Environment*, 41, 3944-3958, 2007.
- 390 Wang, Y. H., Choi, Y. S., Zeng, T., Ridley, B., Blake, N., Blake, D., and Flocke, F.: Late-spring
391 increase of trans-Pacific pollution transport in the upper troposphere, *Geophysical Research*
392 *Letters*, 33, 2006.
- 393 Yang, Q., Wang, Y., Zhao, C., Liu, Z., Gustafson, W. I., and Shao, M.: NO_x Emission Reduction
394 and its Effects on Ozone during the 2008 Olympic Games, *Environ. Sci. Technol.*, 45, 6404-6410,
395 2011.
- 396 Zeng, T., Wang, Y., Chance, K., Blake, N., Blake, D., and Ridley, B.: Halogen-driven low-altitude
397 O₃ and hydrocarbon losses in spring at northern high latitudes, *Journal of Geophysical Research-*
398 *Atmospheres*, 111, 2006.



- 399 Zeng, T., Wang, Y. H., Chance, K., Browell, E. V., Ridley, B. A., and Atlas, E. L.: Widespread
400 persistent near-surface ozone depletion at northern high latitudes in spring, *Geophysical Research*
401 *Letters*, 30, 2003.
- 402 Zhang, Q., Geng, G. N., Wang, S. W., Richter, A., and He, K. B.: Satellite remote sensing of
403 changes in NO_x emissions over China during 1996-2010, *Chin. Sci. Bull.*, 57, 2857-2864, 2012.
- 404 Zhang, Q., Streets, D. G., Carmichael, G. R., He, K. B., Huo, H., Kannari, A., Klimont, Z., Park,
405 I. S., Reddy, S., Fu, J. S., Chen, D., Duan, L., Lei, Y., Wang, L. T., and Yao, Z. L.: Asian emissions
406 in 2006 for the NASA INTEX-B mission, *Atmospheric Chemistry and Physics*, 9, 5131-5153,
407 2009.
- 408 Zhang, Q., Streets, D. G., He, K., Wang, Y., Richter, A., Burrows, J. P., Uno, I., Jang, C. J., Chen,
409 D., Yao, Z., and Lei, Y.: NO_x emission trends for China, 1995-2004: The view from the ground
410 and the view from space, *Journal of Geophysical Research-Atmospheres*, 112, 18, 2007.
- 411 Zhang, Y., Wang, Y., Chen, G., Smeltzer, C., Crawford, J., Olson, J., Szykman, J., Weinheimer,
412 A. J., Knapp, D. J., Montzka, D. D., Wisthaler, A., Mikoviny, T., Fried, A., and Diskin, G.: Large
413 vertical gradient of reactive nitrogen oxides in the boundary layer: Modeling analysis of
414 DISCOVER-AQ 2011 observations, *Journal of Geophysical Research: Atmospheres*, 121,
415 2015JD024203, 2016.
- 416 Zhao, C. and Wang, Y.: Assimilated inversion of NO_x emissions over east Asia using OMI NO₂
417 column measurements, *Geophysical Research Letters*, 36, L06805, 2009.
- 418 Zhao, C., Wang, Y., Choi, Y., and Zeng, T.: Summertime impact of convective transport and
419 lightning NO_x production over North America: modeling dependence on meteorological
420 simulations, *Atmos. Chem. Phys.*, 9, 2009a.
- 421 Zhao, C., Wang, Y., Yang, Q., Fu, R., Cunnold, D., and Choi, Y.: Impact of East Asian summer
422 monsoon on the air quality over China: View from space, *Journal of Geophysical Research:*
423 *Atmospheres*, 115, D09301, 2010.
- 424 Zhao, C., Wang, Y. H., and Zeng, T.: East China Plains: A "Basin" of Ozone Pollution, *Environ.*
425 *Sci. Technol.*, 43, 1911-1915, 2009b.



426



427

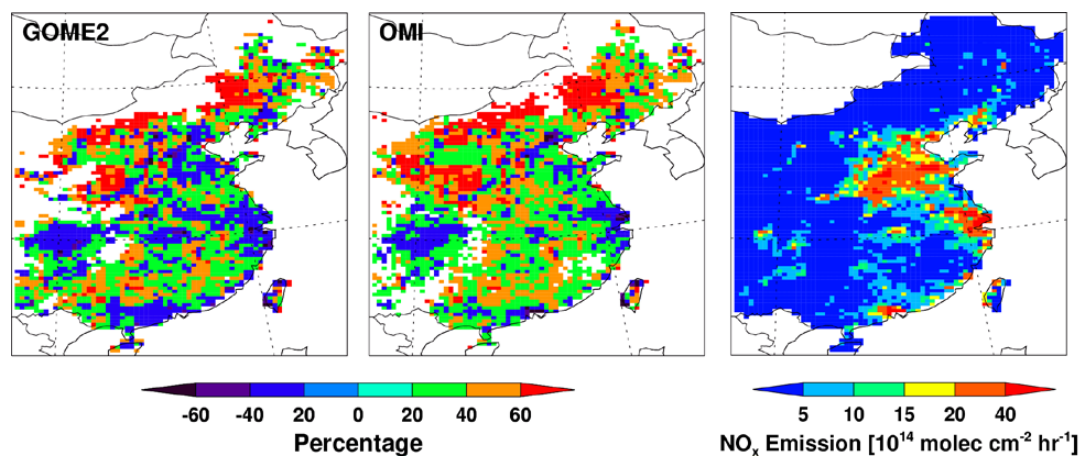
428 Figure 1. Simulated NO₂ column density as a function of surface NO_x emission at GOME-2 (black)
429 and OMI (yellow) overpass time over eastern China for August, 2007. The dots are grid average
430 data from REAM simulations binned by an emission interval of 1×10^{14} molec cm⁻² and the solid
431 lines are from least-square polynomial regression results.

432

433

434

435



436

437 Figure 2. Relative difference between monthly mean local derivative ratio α^* and bulk ratio α ,
438 defined as $1 - \alpha/\alpha^*$, for GOME-2 (left) and OMI (middle) in REAM simulations. The right panel
439 shows NO_x emission distribution estimated from GOME-2 observations by using the local
440 derivative method over eastern China for August 2007.

441

442

443

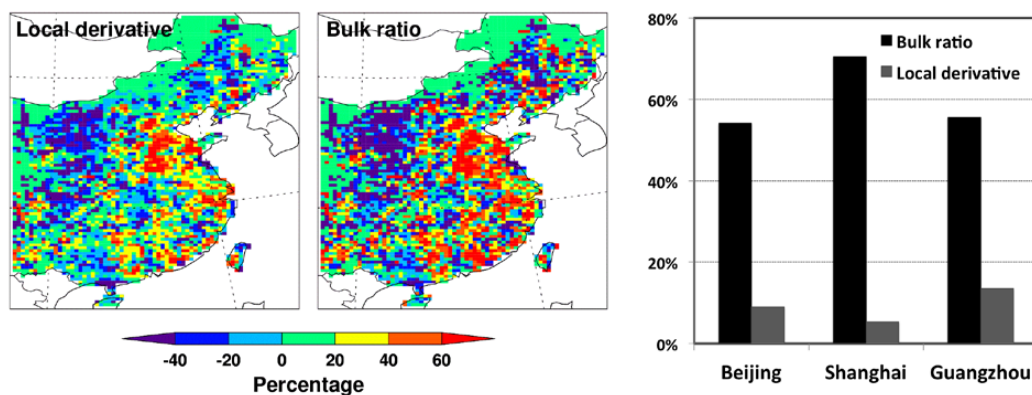
444

445

446

447

448

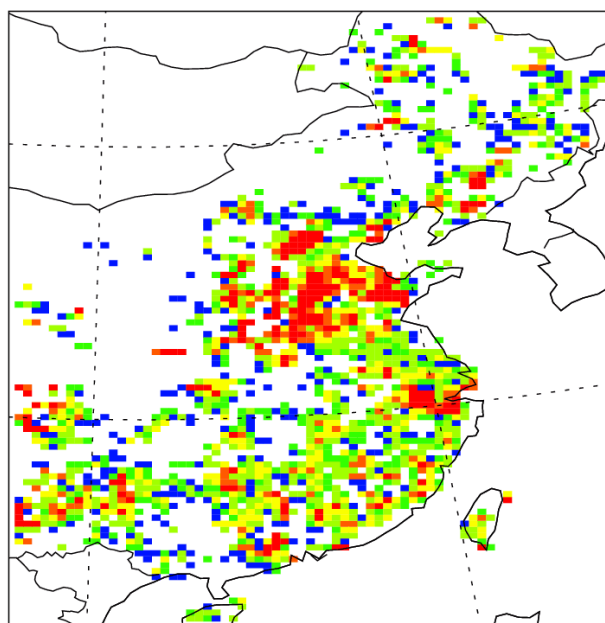


449

450 Figure 3. Relative difference of inversion emission estimates for NO_x with GOME-2 relative to
451 OMI products using the local derivative and the bulk ratio methods: regional distributions over
452 eastern China, respectively, for August 2007 (left), and the differences in three megacities (right).

453

454



Delta Ratio of NO₂ columns

455

456 Figure 4. The distribution of $(\Omega_{\text{GOME-2}}/\Omega_{\text{m0930}}) - (\Omega_{\text{OMI}}/\Omega_{\text{m1330}})$ over eastern China for August 2007.

457

458

459

460

461

462

463

464

465

466

467



468 Table 1. NO_x inversion emission estimates the using the local derivative, bulk ratio, and satellite
 469 differential inversion methods

Method		Emission Rate (10 ¹⁵ molec. cm ⁻² hr ⁻¹)			Total Emission of East China (Tg N yr ⁻¹)
		Beijing	Shanghai	Guangzhou	
Local derivative	GOME-2	7.78	13.8	4.71	6.18
	OMI	7.14	13.1	4.15	5.82
Bulk ratio	GOME-2	6.86	12.62	8.68	6.13
	OMI	4.45	7.40	5.58	5.50
Satellite differential		3.31	7.19	4.32	5.26
A priori estimates		9.68	16.9	4.76	5.27

470

471